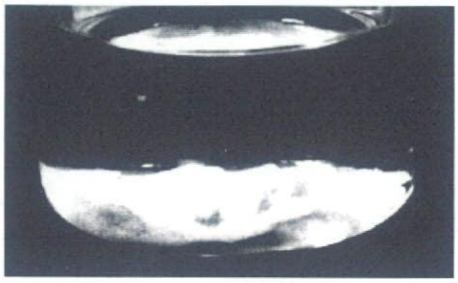

Figure 3. 3DP block in water. It was found to be soluble easily.

The solubility test analysis had shown the quantity of calcium ions (Table I).

From the result of ICP analysis, it is obvious that the amount of calcium ion in the solution drops from 199 to 34.5 mg/L after heated at 300°C for 10–30 min. However, after heated at 300°C for 30 min, the physical properties of the samples were unacceptably weak. The insolubility test reveals that heat treatment at 300°C for 10 min yield the best condition of insolubilized samples.

TABLE I. Solubility Test Analysis of Calcium Ions in the Specimen

Treatment condition of 3DP samples	Amount of Ca^{2+} in the solution (mg/L)	Visual examination
Not treated 3DP sample	189	Dissolved in water
100°C 30 min heated	158	Slightly change in color, dissolved in water
200°C 30 min heated	199	Slightly change in color, dissolved in water
300°C 10 min heated	34.5	Dark color, not dissolved in water
300°C 30 min heated	36.8	Dark color with ashes, not dissolved in water but broke easily into 2 parts

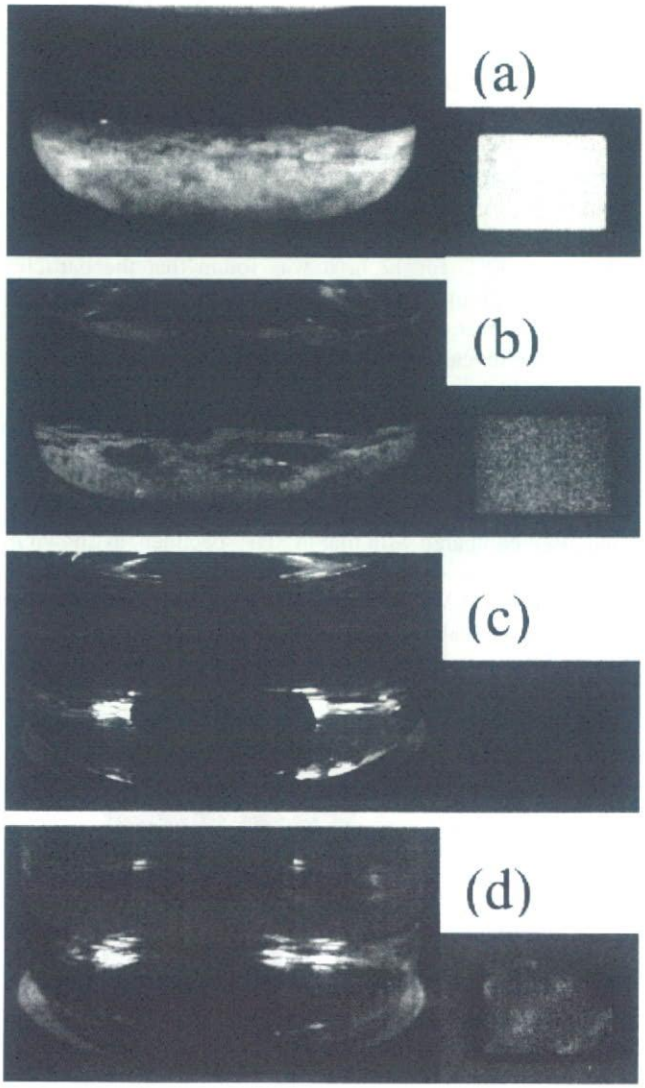

Figure 4. Solubility test of heated 3DP blocks at different temperatures: (a) after heated at 100°C for 30 min, (b) after heated at 200°C for 30 min, (c) after heated at 300°C for 10 min, (d) after heated at 300°C for 30 min.

XRD Analysis of 3DP and POP Blocks After Treatment in Ammonium Phosphate Solution

All specimens including POP were immersed in ammonium phosphate solution, and the transformation by treatment was examined by XRD. Figure 5 shows XRD patterns of fabricated 3DP block before and after various treatments. The peaks of gypsum dihydrate ($CaSO_4 \cdot 2H_2O$) were exclusively observed before the treatment [Figure 5(a)]. After the heat

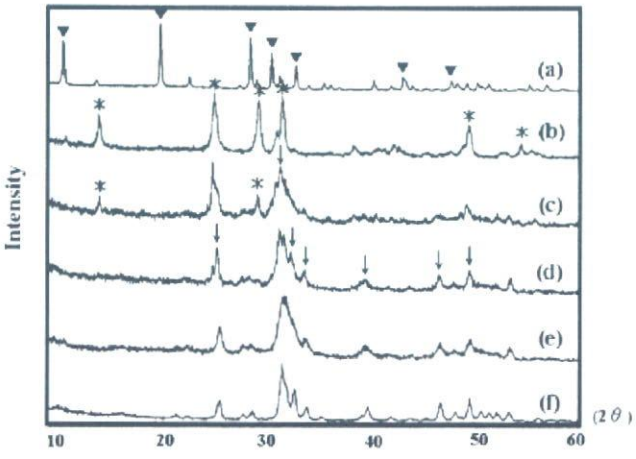

Figure 5. XRD pattern of 3DP blocks: (a) untreated 3DP block, (b) 3DP block after heat treatment at 300°C for 10 min, (c) heated 3DP block after immersion in $(NH_4)_3PO_4$ for 1 h, (d) heated 3DP block after immersion in $(NH_4)_3PO_4$ for 4 h, (e) heated 3DP block after immersion in $(NH_4)_3PO_4$ for 8 h, and (f) HA. Crystallization of the specimen: ▼ = $CaSo_4.2H_2O$, * = $CaSo_4.1/2H_2O$, ↓ = HA.

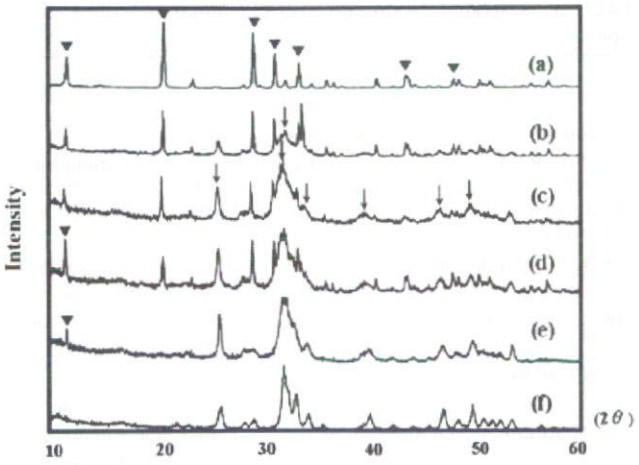

Figure 6. XRD pattern of plaster of Paris: (a) POP blocks, (b) POP block after immersion in $(NH_4)_3PO_4$ for 1 h, (c) POP block after immersion in $(NH_4)_3PO_4$ for 4 h (d) POP block after immersion in $(NH_4)_3PO_4$ for 12 h, (e) POP block after immersion in $(NH_4)_3PO_4$ for 24 h, and (f) HA. Crystallization of the specimen: ▼ = $CaSo_4.2H_2O$, ↓ = HA.

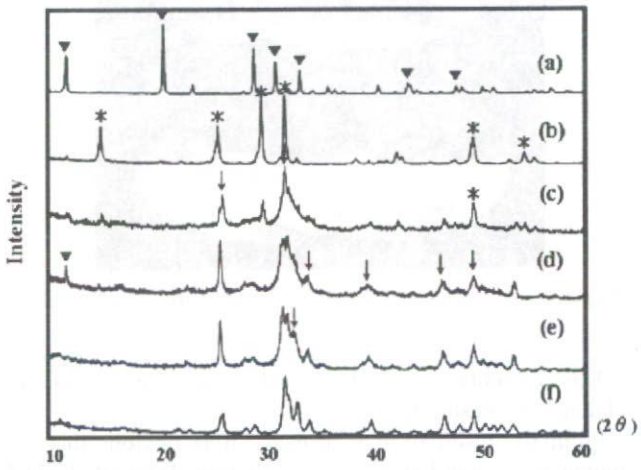

Figure 7. XRD pattern of plaster of Paris heated at 300°C: (a) POP block, (b) POP block heated at 300°C for 10 min, (c) heated POP block after immersion in $(NH_4)_3PO_4$ for 1 h, (d) heated POP block after immersion in $(NH_4)_3PO_4$ for 4 h, (e) heated POP block after treatment in $(NH_4)_3PO_4$ for 24 h, and (f) HA. Crystallization of the specimen: ▼ = $CaSo_4.2H_2O$, * = $CaSo_4.1/2H_2O$, ↓ = HA.

treatment for insolubilization at 300°C for 10 min, the XRD pattern revealed the peaks of calcium sulfate hemihydrate ($CaSO_4 \cdot 0.5H_2O$) [Figure 5 (b)]. After 1 h treatment in 1*M* $(NH_4)_3PO_4 \cdot 3H_2O$ solution at 80°C, the XRD pattern had shown several peaks assigned to HA, besides the hemihydrate peaks [Figure 5(c)]. After immersion in the solution for 4 and 8 h, the hemihydrate peaks disappeared, and only HA peaks were observed [Figure 5(d,e)].

Figure 6 shows the XRD pattern of POP block treated in the solution in the same way as the 3DP block. It was found that HA formation by the treatment in the phosphate solution at 80°C proceeded slower than the 3DP specimens. After treatment for 1 h, the peak intensity of gypsum decreased, and formation of HA was also confirmed by the peak around 32° [Figure 6(b)]. After treatment for 4 and 12 h, the XRD pattern showed more peaks of HA though a small amount of gypsum still remained for 24 h [Figure 6(c–e)]. Transformation of gypsum to HA was almost completed after the treatment for 24 h, but trace amount of gypsum was still observed [Figure 6(e)].

Figure 7 shows the XRD pattern of plaster of Paris heated at 300°C for 10 min and treated in the phosphate solution. After heat treatment, gypsum was transformed into hemihydrate [Figure 7(b)]. After 1 h of treatment in the phosphate solution, the XRD pattern clearly showed formation of more HA than that in the unheated specimen [Figures 6(b) and 7(c)]. After 4 h of immersion, the XRD pattern shows HA as a main product together with a small amount of gypsum as byproduct. After 24 h of treatment, the XRD pattern revealed only a HA profile. However, the specimens became fragile and brittle after immersion in the solution at 80°C, as shown in Figure 8.

Scanning Electron Microscopy

Figure 9 shows SEM photographs of surfaces of the 3DP and POP specimens after various treatments. The surface of the 3DP specimen before the treatment shows the grains with spongy and irregular shapes [Figure 9(a,b)]. After immersion of the heat-treated 3DP specimen in ammonium phosphate solution at 80°C for 12 h, it was found that the particles cluster into groups and yield the widening interspaces at lower magnification [Figure 9(c)]. A higher magnification SEM image reveals needle-like crystals on the surface of the particles, which are typical for HA crystals projected from the surfaces of particles [Figure 9(d)]. On the other hand, crystals with rod and regular shapes are seen on the surface of the POP specimen treated in ammonium phosphate solution at 80°C for 24 h. The arrangement of the crystals is more condensed compared with that in 3DP specimen, as shown in the low magnification SEM image [Figure 9(c,e)]. Higher magnification SEM image reveals the formation of smaller needle-like crystals in the POP specimen than in the 3DP specimen [Figure 9(d,f)]. The SEM images of the heat-treated

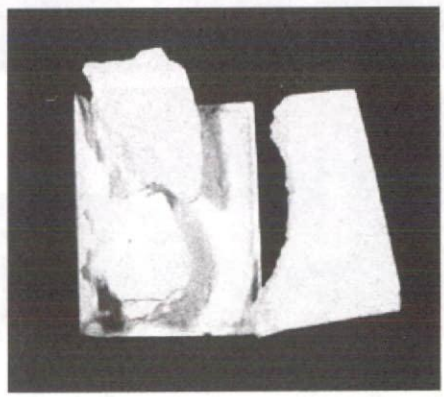

Figure 8. Heated POP block treated in ammonium phosphate solution at 80°C for 24 h. Specimen became fragile and brittle.

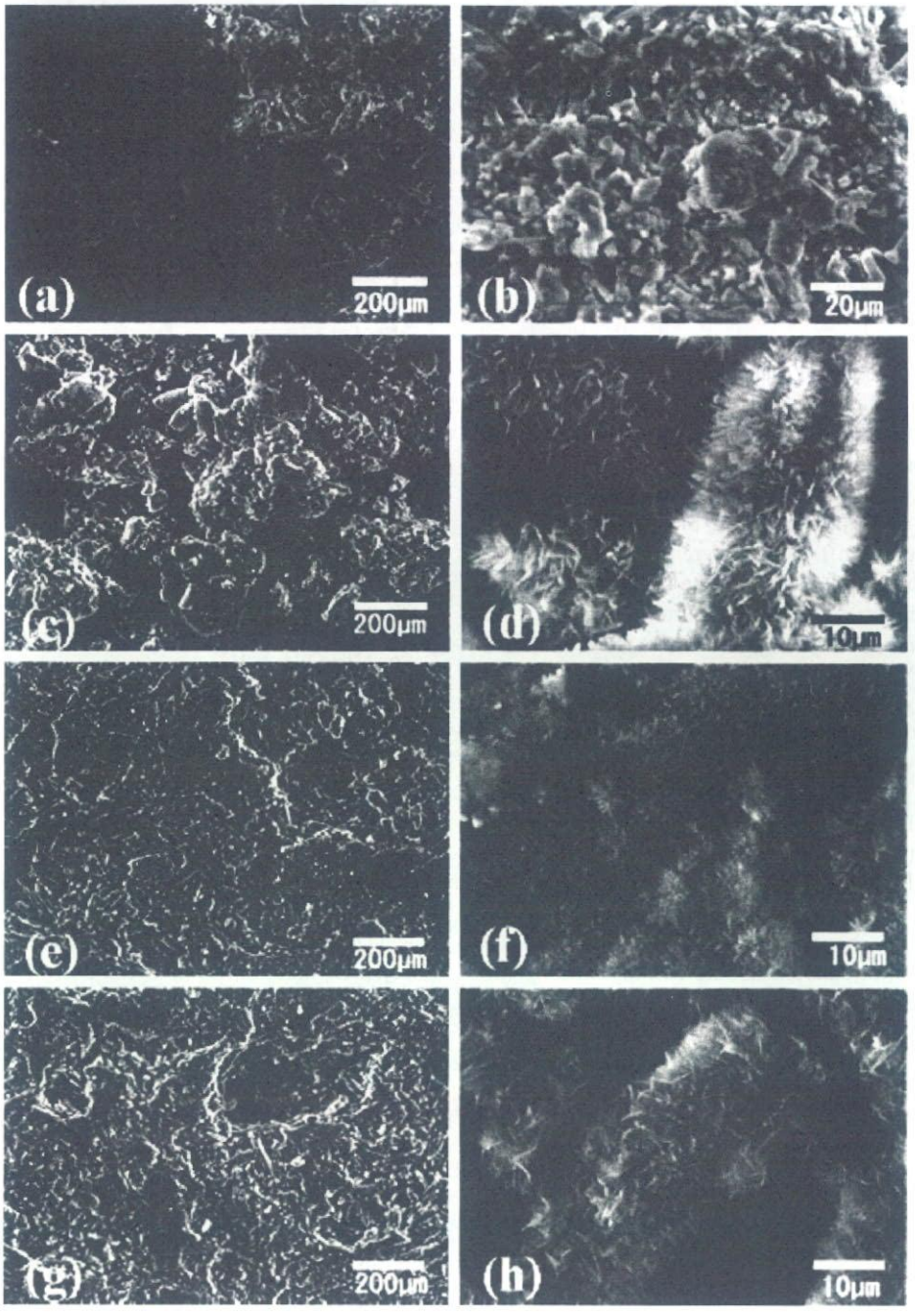

Figure 9. Scanning electron microscopy of surface (a,b) fabricated 3DP block, (c,d) 3DP block heated 300°C for 10 min and treated in ammonium phosphate solution at 80°C for 12 h, (e,f) POP block treated in ammonium phosphate solution at 80°C for 24 h, (g,h) 300°C for 10 min heated POP block treated in ammonium phosphate solution at 80°C for 24 h.

POP specimen after treatment in ammonium phosphate solution at 80°C for 24 h are shown in Figure 9(g,h). The low-magnification SEM image shows more porous and condensed structure of rod-shaped particles compared with that of the unheated POP. Higher-magnification SEM picture illustrates the larger needle-like crystals on the surface of the particles and wider inter-crystal spaces than the unheated POP. The needle-like crystals are about the same size as in the heated 3DP specimen [Figure 9(d,h)].

DISCUSSION

We could obtain an insoluble 3DP block by heat treatment at 300°C. However, the color of the block turned to be dark

brown, as shown in Figure 4(c,d). Then, we have examined additionally FTIR analysis (FTIR-8300, Shimadzu, Kyoto, Japan) of the ink used for the 3D printing before and after heating. Before heating, it showed the pattern similar to glycerin, with some strong absorption at about 1300 cm^{-1}, where is the C—C bond. After heating, the absorption of almost the same wave number was observed. Accordingly, the brown color resulted from burning of the glycerin in the specimens. Though the mechanism of insolubilization of the 3DP specimen is not clear, it is probably related to adhesive coating on the 3DP hemihydrate powder by heated glycerin.

When the 3DP specimen was treated in the ammonium phosphate solution, we found that the 3DP block was transformed to HA much faster than the POP block. The XRD pattern of 3DP block showed a quick transformation to HA after treatment for only 1 h, and the transformation was almost completed within 4 h [Figure 5(c,d)]. However, gypsum still remained in the unheated POP block, even after 24 h of treatment [Figure 6(e)]. The difference in the rate of transformation is probably caused by the fact that the initial crystal phase of heat-treated 3DP block after insolubilization was calcium sulfate hemihydrate as shown in Figure 5(b) whereas that of POP was gypsum dihydrate as shown in Figure 6(a). It is well known that hemihydrate had four times higher solubility than gypsum dihydrate,[16] and the higher solubility made it easy to transform to HA in the phosphate solution.

The difference in transformation rate may be caused by a difference in existing phase before treatment in the solution. Accordingly, the POP specimen underwent the same heat treatment at 300°C for 10 min as the 3DP block to confirm the above hypothesis. As shown in Figure 7(b), gypsum in the specimen changed into calcium sulfate hemihydrate by the heat treatment, and it transformed into HA much faster than the untreated POP block [Figures 6(c) and 7(d)].

The porosity of 3DP block also accelerates the transformation to HA. To examine the HA transformation inside the block, half of the specimen's thickness was removed and analyzed using XRD. The XRD of 3DP block showed complete HA transformation in the deeper layer (about 2 mm) after 8 h of treatment [Figure 10(a)] compared with the XRD of heated POP treated in ammonium phosphate for 8 h [Figure 10(b)], in which the XRD pattern was mainly gypsum hemihydrate.

SEM observation revealed that the 3DP block was more porous than the unheated POP block. The less porosity in the POP block hindered a penetration of the phosphate solution inside the block and limited the formation of HA only in the surface region, which made it more difficult for the solution to penetrate further. This was also confirmed by the fact that the 3DP block had a smaller apparent density than the POP block because of porosity. The average density of each group of 12 samples was 0.95 ± 0.017 g/cm^3 for 3DP blocks and 1.4 ± 0.047 g/cm^3 for POP blocks, respectively. The density of POP block group was found to be significantly higher than 3DP block group, yielding the lower porosity of POP blocks than that of 3DP samples. Therefore, complete HA transformation inside 3DP block can be seen whereas the transformation of POP block had occurred well near the block surface.

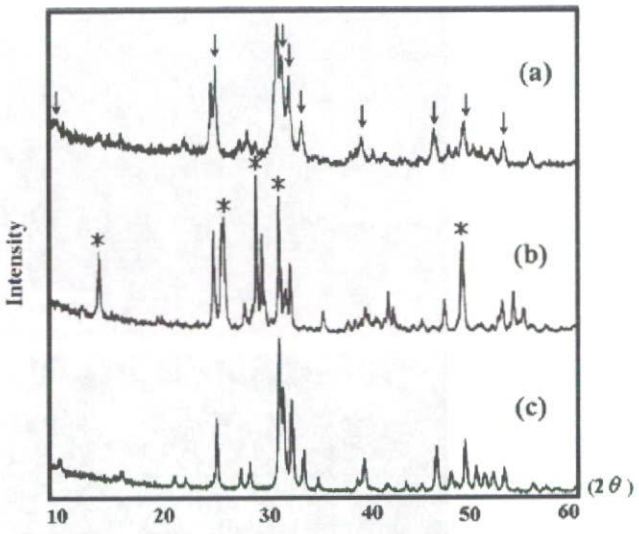

Figure 10. The XRD pattern of (a) 3DP specimen in the depth of about 2 mm treated in ammonium phosphate solution for 8 h. The data has shown complete HA transformation; (b) 300°C heated POP block in the depth of about 2 mm treated in ammonium phosphate solution for 8 h; and (c) HA. Crystallization of the specimen: * = $CaSo_4.1/2H_2O$, ↓ = HA.

Since the 3DP technique can fabricate any prototype part directly from a CAD model, a gypsum model of human jaw bone was fabricated from 3D-CT image. The gypsum model was heat treated at 300°C for 10 min and then treated in 1*M* $(NH_4)_3PO_4$ solution at 80°C for 24 h. Figure 11 shows the bone model consisting of HA fabricated by the above procedure. Though full jaw bone model may not be required in the clinical application, a proposed 3DP method in the present study can be a tool to fabricate the scaffold that fits to the bone defects in the fields of orthopedics and oral maxillofacial surgery. The architectures of scaffold also influence the pattern of bone growth and effective tissue engineering treatment. Recently, solid freeform fabrication (SFF) has played important roles in the fabrication of negative mold with desirable architecture. Fuse deposition modeling systems, an example of SFF, allow the fabrication of a mold from wax materials, which is easily removed by low temperature.[9] The indirect wax mold can also be obtained by 3DP technique[8] which can be applied with assorted scaffold designs, materials, and casting method. Roy et al.[7] reported the fabrication of HA scaffold via direct 3DP technique. The binder was specially formulated for the 3DP fabrication, and finally, sintering process was acquired to burn out the binder. Even though sintering process can retain the shape of HA cements or powders and yield the stronger and stiffer ceramic, it brings about the inconvenience that they are not degradable in the appropriate time. This technique of direct 3DP should eliminate the difficulty in trimming the HA block scaffold and has a great potential for fabrication of HA scaffold with desirable

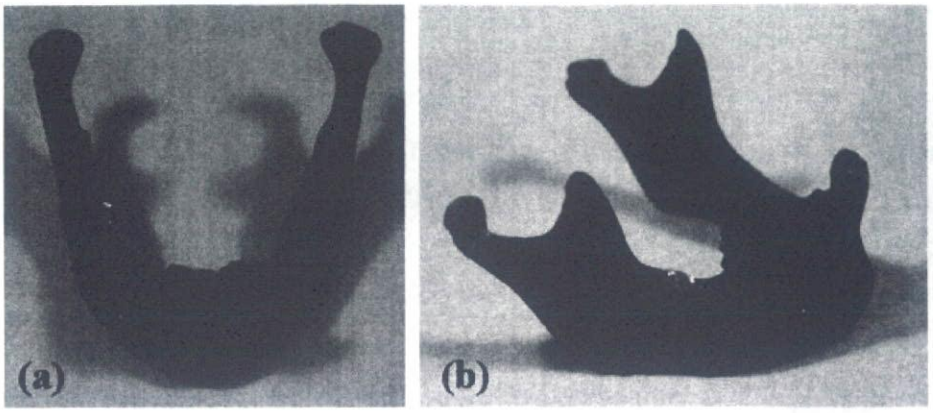

Figure 11. 3DP model of mandible treated in ammonium phosphate solution at 80°C for 24 h. (a) Frontal view and (b) lateral view.

internal structure that avoids sintering process. For future study, we would like to focus on the method for strength improvement of other biocompatible materials that can be fabricated by direct 3DP technique.

We thank to Kansai Polytechnic Center for fabrication of 3DP specimens and Professor Kenjiro Oura and Ms. Winadda Wongwiriyapan Faculty of Engineering, Osaka University for their assistance in SEM observation.

REFERENCES

1. Tieliewuhan Y, Hirata I, Sasaki A, Minagi H, Okazaki M. Osteoblast proliferation behavior and bone formation on and in Co_3 apatite-collagen sponges with a porous hydroxyapatite frame. Dent Mater J 2004;23:258–264.
2. Mimura K, Watanabe K, Okawa S, Kobayashi M, Miyakawa O. Morphological and chemical characterizations of the interface of a hydroxyapatite-coated implant. Dent Mater J 2004;23:353–360.
3. Doi Y, Shibutani T, Moriwaki Y, Kajimoto T, Iwayama Y. Sintered carbonate apatites as bioresorbable bone substitutes. J Biomed Mater Res 1998;39:603–610.
4. Schmitz JP, Hollinger JO, Milam SB. Reconstruction of bone using calcium phosphate bone cement: A critical review. J Oral Maxillofac Surg 1999;57:1122–1126.
5. Barralet JE, Grover L, Gaunt T, Wright AJ, Gibson IR. Preparation of macroporous calcium phosphate cement tissue engineering scaffold. Biomaterials 2002;23:3063–3072.
6. Mooney V, Massie J, Lind BI, Rah JH, Negri S, Holmes RE. Comparison of hydroxyapatite granules to autogenous bone graft in fusion cages in a goat model. Surg Neurol 1998;49:628–634.
7. Roy TD, Simion LJ, Ricci JL, Rekow ED, Thompson VP, Parsons JR. Performance of hydroxyapatite bone repair scaffolds created via three-dimensional fabrication techniques. J Biomed Mater Res A 2003;67:1228–1237.
8. Taboas JM, Maddox RD, Krebsbach PH, Hollister SJ. Indirect solid free form fabrication of local and global porous, biomimetic and composite 3D polymer-ceramic scaffolds. Biomaterials 2002;24:181–194.
9. Charrière E, Lemaitre J, Zysset Ph. Hydroxyapatite cement scaffolds with controlled macroporosity: Fabrication protocol and mechanical properties. Biomaterials 2003;24:809–817.
10. Tadic D, Beckmann F, Schwarz K, Epple M. A novel method to produce hydroxyapatite objects with interconnecting porosity that avoids sintering. Biomaterials 2004;25:3335–3340.
11. Bahn SL. Plaster: A bone substitute. Oral Surg Oral Med Oral Pathol 1966;21:672–681.
12. Peltier LF. The use of plaster of Paris to fill defects in bone. Clin Orthop 1961;21:1–31.
13. Frame JW. Porous calcium sulfate dihydrate as biodegradable implant in bone. J Dent 1975;3:177–187.
14. Sato S, Koshino T, Saito T. Osteogenic response of rabbit tibia to hydroxyapatite particle-plaster of Paris mixture. Biomaterials 1998;19:1895–1900.
15. Suzuki Y, Matsuya S, Udoh K, Nakagawa M, Koyano K, Ishikawa K. Fabrication of hydroxyapatite monolith from gypsum with the presence of ammonium phosphate. Arch Bioceram Res 2003;3:77–82.
16. Kenneth JA, Ralph WP. Phillips's Science of Dental Materials, 10th ed. Philadelphia: Saunder; 1996. pp 188, 189.

J Mater Sci (2007) 42:5728–5735
DOI 10.1007/s10853-006-0747-7

Development of macropores in calcium carbonate body using novel carbonation method of calcium hydroxide/sodium chloride composite

Yoong Lee · Yeong Min Hahm · Shigeki Matsuya · Masaharu Nakagawa · Kunio Ishikawa

Received: 25 January 2006 / Accepted: 1 August 2006 / Published online: 21 April 2007

Abstract Calcium carbonate is one of the bioceramics and has been used clinically as a bone substitute in dental and orthopedic surgery. Introduction of macropores into the bioceramics is highly recommended because those pores enable tissue ingrowth and accelerated osteointegration. We tried to prepare calcium carbonate body with macropores through the new carbonation method of calcium hydroxide/sodium chloride composite. Sodium chloride acted as a water-soluble porogen in developing macropores in calcium carbonate body and was removed completely by washing with distilled water after carbonation. We investigated effects of sodium chloride content and molding pressure on the porosity and the mechanical strength of the calcium carbonate body. Through this study, it was found that the porosity of body increased with the sodium chloride content in composite and was hardly affected by molding pressure. On the other hand, the mechanical strength was increased with the molding pressure and reduced with the porosity. In addition, the increase in content of sodium chloride caused the enlargement of hole size as well as the enhancement of extent of interconnection among pores through hole. Especially, the calcium carbonate body with over 90% porosity could be prepared when 90 wt.% sodium chloride was used under 10 MPa molding pressure. Its average pore and hole size were 177 and 80 μm, respectively.

Y. Lee · S. Matsuya · M. Nakagawa · K. Ishikawa
Department of Biomaterials, Faculty of Dental Science, Kyushu University, 3-3-1 Maidashi, Higashiku, Fukuoka 812-8582, Japan

Y. Lee (✉) · Y. M. Hahm
Department of Chemical Engineering, College of Engineering, Dankook University, Seoul 140-714, Korea
e-mail: ly02147@gmail.com

Introduction

Bioceramics in biomaterial fields have been developed to replace osseous tissues and complete autografts and allografts. Many researches with respect to them have been placed on the fabrication of bioceramics with porous configuration [1–5].

Calcium carbonate ($CaCO_3$), which is biocompatible and biodegradable, can be used not only as a bioceramic itself but as a precursor of carbonate apatite which is analogous to the inorganic component of vertebrate's hard tissue [3, 6–8]. Although several methods for the preparation of $CaCO_3$ have been reported, they are mostly concerned with the fabrication of its powder [9–12]. Even if it has been fabricated in the form of cylinder or other shape, there have been very a few active efforts to develop appropriate pore or to enhance porosity until now [3, 13].

The pore size and porosity of bioceramics play an important role in tissue ingrowth with an internal surface area available for cell adhesion, spreading and expansion, adsorption of biologic metabolites, and resorbability at controlled rates to match that of tissue repair [14]. It is generally accepted that if the pore size is in the range of 100–400 μm, this macropore allows bone tissue ingrowth, making direct integration with bone to improve the mechanical fixation of the implant at the implantation site and nutrient delivery to the center of the regenerated tissue [15–17]. When an implanted macroporous bioceramic is progressively replaced by natural bone, its biomechanical properties resemble more and more those of natural bone [15].

The impregnation and gel-casting of foams, the inclusion of porogenic volatile or soluble substances, and the dual phase mixing have been proposed for the development of macropores in bioceramics [3, 18–21]. However, a high temperature treatment employed by the most of these methods is not suitable for the fabrication of macroporous $CaCO_3$ body because it decomposes into calcium oxide (CaO) and carbon dioxide (CO_2) at high temperature [22]. In our previous work [23], we have already introduced the novel method of fabrication of pure $CaCO_3$ block using the carbonation of calcium hydroxide block at room temperature. Moreover, the low temperature processing enables addition of different kinds of proteins, antibiotics, antiinflamatory, anticancer drugs, etc into the material [24–27].

The present study reports the method of preparation of macroporous calcium carbonate body using sodium chloride as a porogen by previously reported carbonation method. In order to impart mechanical strength to macroporous calcium carbonate body we applied molding pressure while preparing calcium hydroxide/sodium chloride composite. The change of NaCl content and molding pressure were chosen as experimental parameters and experiments were designed to achieve: increase in the porosity under a low molding pressure, enhancement of the mechanical strength under constant sodium chloride content and increase in the porosity of the body under high molding pressure. It was investigated how degree of carbonation, pore and hole size formed in pores, porosity, and mechanical strength of body are affected by the experimental parameters.

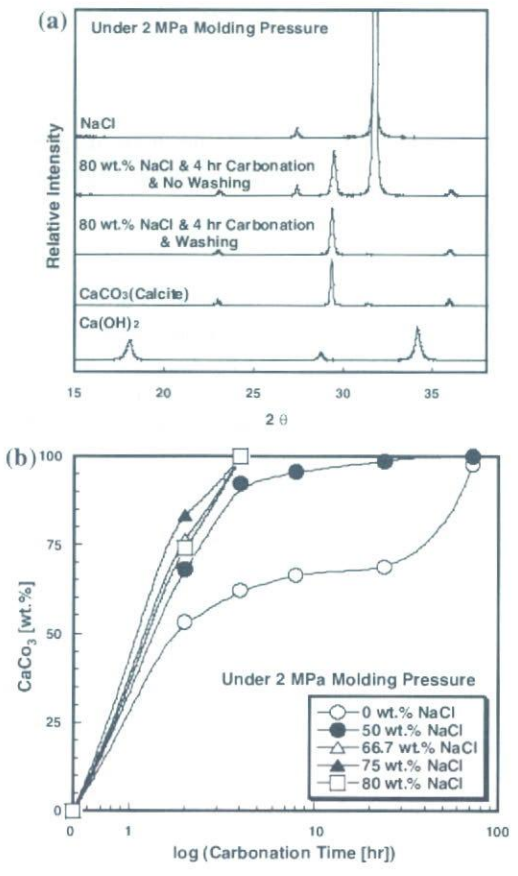

Fig. 1 (**a**) Powder XRD patterns of the $Ca(OH)_2$/NaCl composite containing 80 wt.% NaCl prepared at 2 MPa molding pressure after 4 h carbonation. (**b**) Changes of $CaCO_3$ content in the $Ca(OH)_2$/NaCl composites with carbonation time at various NaCl content under 2 MPa molding pressure

Materials and methods

Preparation of calcium hydroxide/sodium chloride composite

Calcium hydroxide ($Ca(OH)_2$; Wako Chemicals, Osaka, Japan) and sodium chloride (NaCl; Wako Chemicals, Osaka, Japan) were used for the present study. The particle size distribution of $Ca(OH)_2$ with irregular shape was from submicron to several micron. NaCl was pulverized mechanically and sieved to obtain 106–300 μm particulates before used. A variety of mixtures were prepared manually using 0.2 g $Ca(OH)_2$ and NaCl in the 0–90 wt.% range. Each mixture was subject to pressure uniaxially in stainless steel die of 10 mm in inner diameter using an oil pressure press machine (Riken Power, Riken Seiki, Japan) at the molding pressure of 2–10 MPa to prepare $Ca(OH)_2$/NaCl composite.

Carbonation and washing of $Ca(OH)_2$/NaCl composite

The composites were carbonated in carbon dioxide reaction vessel for 2–72 h at room temperature. The reaction vessel, approximately 5 l, was saturated with water vapor and carbon dioxide gas was supplied at a rate of 0.15–0.2 l/min. Subsequently, the composites carbonated were washed sufficiently with distilled water at 60 °C for 24 h to drive off NaCl completely and dried at 60 °C for 24 h.

Characterization

Mechanical testing

The mechanical strengths of composites after carbonation and washing were evaluated in terms of diametral tensile strength (DTS) at room temperature at a constant crosshead rate of 1 mm min^{-1} on an universal testing machine

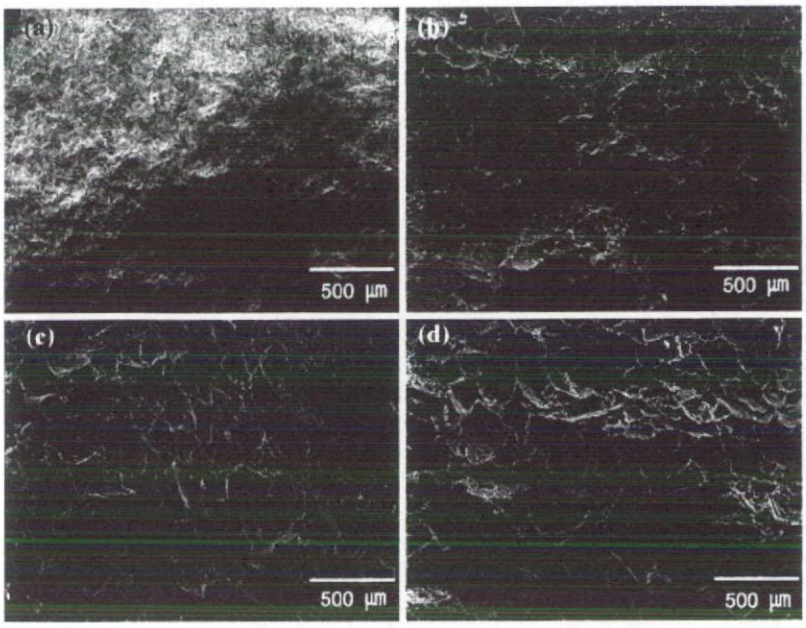

Fig. 2 Scanning electron microscopic observation of the fracture surfaces of $CaCO_3$ bodies under 2 MPa molding pressure. (**a**) 0 wt.% NaCl & 72 h carbonation (**b**) 66.7 wt.% NaCl & 8 h carbonation (**c**) 75 wt.% NaCl & 8 h carbonation (**d**) 80 wt.% NaCl & 8 h carbonation

(SV–301, IMADA, Toyohashi, Aichi, Japan). Five samples were tested for each experimental condition.

X-ray diffraction analysis

The composites after carbonation or carbonation and washing were ground into fine powders. X-ray diffraction (XRD) analysis was carried out using these powders. The XRD patterns were recorded with vertically mounted diffractometer system (RINT 2500 V, Rigaku, Tokyo, Japan) using counter-monochromatized CuKα radiation generated at 40 KV and 100 mA. They were scanned in the range of 2θ from 10 to 60° in a continuous mode at a scanning rate of 2° min^{-1}. Quantitative analysis was also done during carbonation. Calibration curve for the quantitative analysis was made using separated diffraction peaks of $Ca(OH)_2$(001, d = 4.905 Å) and calcite(0–22, d = 2.095 Å), respectively.

Morphology analysis

The morphologies of fracture surfaces of the composites after carbonation and washing were examined by means of a scanning electron microscope (SEM, JSM 5400LV, JEOL, Tokyo, Japan) at an acceleration voltage of 15 kV after gold coating. The average NaCl-print size that can be attributed to the pore size existing in the body and hole size formed in pore were analyzed by means of image analysis software (USB Digital Scale V1.0, Scalar Corporation).

Porosity measurement

The apparent densities of the composites after carbonation and washing were calculated from their weight and dimensions. The relative density was calculated by the ratio of the apparent density to the theoretical density of calcite (2.711 g cm^{-3}). The total porosity of the body is defined as follows;

$$\text{Total porosity}(\%) = 100(\%) - \text{relative density}(\%)$$

The total porosity was the average value of five bodies.

Results and discussion

Effect of NaCl content under 2 MPa molding pressure

Figure 1a is the XRD patterns of the composite obtained from the $Ca(OH)_2$/80 wt.% NaCl composite carbonated for 4 h before and after washing with distilled water at 60 °C. It confirms that NaCl was removed totally through washing and $CaCO_3$ body with calcite phase was formed completely within this carbonation time. Figure 1b shows the degree of carbonation of the composites in terms of NaCl content and

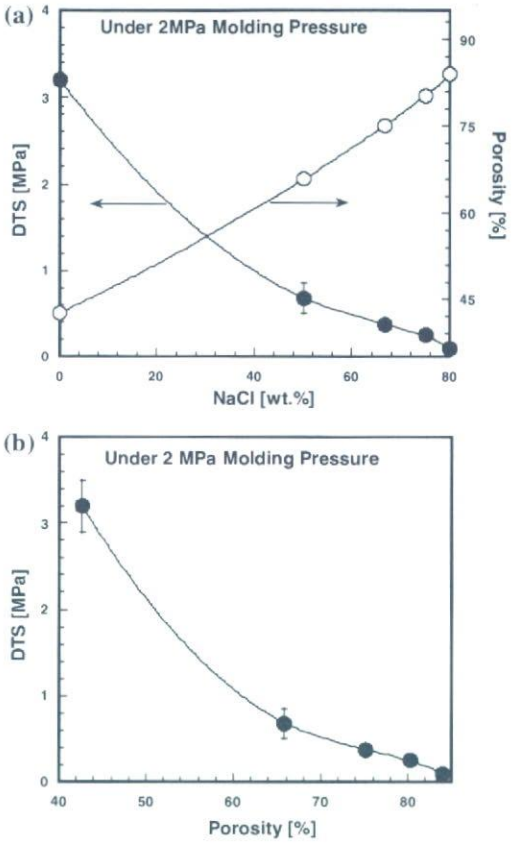

Fig. 3 (**a**) Changes in diametral tensile strengths and porosities of $CaCO_3$ bodies with NaCl content under 2 MPa molding pressure. (**b**) Changes in diametral tensile strengths of $CaCO_3$ bodies with porosity under 2 MPa molding pressure

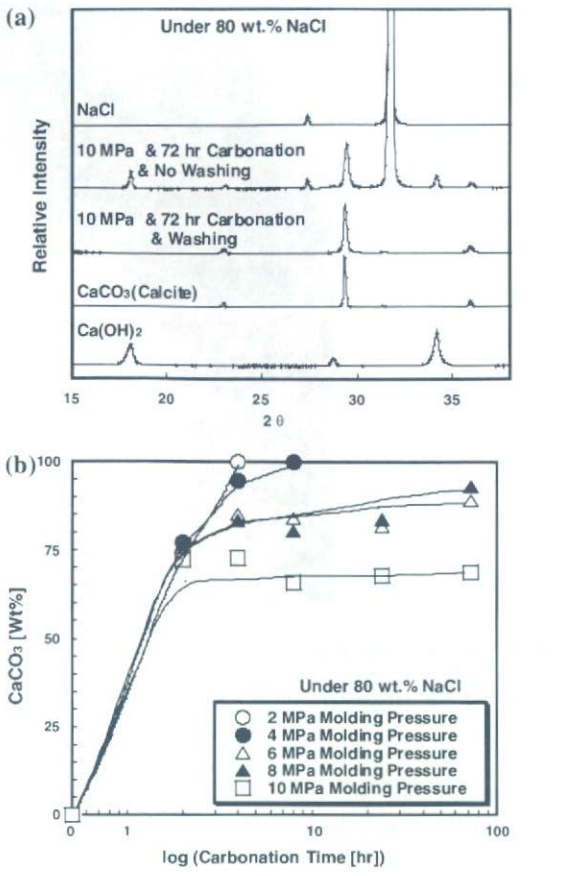

Fig. 4 (**a**) Powder XRD patterns of the $Ca(OH)_2$/NaCl composite containing 80 wt.% NaCl prepared at 10 MPa molding pressure after 72 h carbonation. (**b**) Changes of $CaCO_3$ content in the $Ca(OH)_2$/NaCl composites with carbonation time at various molding pressure under 80 wt.% NaCl

carbonation time. The time required to transform $Ca(OH)_2$ into $CaCO_3$ reduced with the increase in NaCl content. When the composite was prepared using more than 66.7 wt.% NaCl, $Ca(OH)_2$ was transformed into $CaCO_3$ within 4 h. Whereas, carbonation was remarkably delayed and completed after 72 h for the pure $Ca(OH)_2$ body.

The carbonation of $Ca(OH)_2$ is expressed as the following reaction:

$$Ca(OH)_2 + CO_2 \leftrightarrow CaCO_3 + H_2O$$

CO_2 gas is absorbed in water and NaCl has the property of adsorbing water [28–30]. Consequently, the composites with NaCl get carbonated faster than that without NaCl, because NaCl adsorbs moisture existing in the reaction vessel and this moisture dissolves CO_2 gas, promoting the opportunity of contacting CO_2 with $Ca(OH)_2$. Therefore, the acceleration in carbonation can be attributed to the ability of water adsorbance by NaCl and dissolution of CO_2 into water, which is directly proportional to NaCl content under this molding pressure (Fig. 1b).

Figure 2 shows the SEM images of fracture surfaces of $CaCO_3$ bodies after carbonation and washing. The fracture surface of the body prepared without using NaCl was dense and compact at this magnification level (Fig. 2a), while NaCl-prints on the bodies prepared using NaCl can be seen clearly (Fig. 2b–e). The NaCl-print size can be attributed to pore size existed in the body and some pores were interconnected through holes that can be revealed from black part in the pores. The degree of existence of pores and interconnection among them augmented more and more with the increase in NaCl content. In case of the body prepared using 80 wt.% NaCl, the average pore size and hole size were 160 and 49 μm, respectively.

Figure 3a shows the change in the porosity and the mechanical strength of the $CaCO_3$ bodies with NaCl content after carbonation and washing. In case of porosity, it was almost linearly increased in proportion to NaCl content. When body was prepared using 80 wt.% NaCl, the porosity was 84%, which is higher than any other body prepared under this experimental condition. However, as

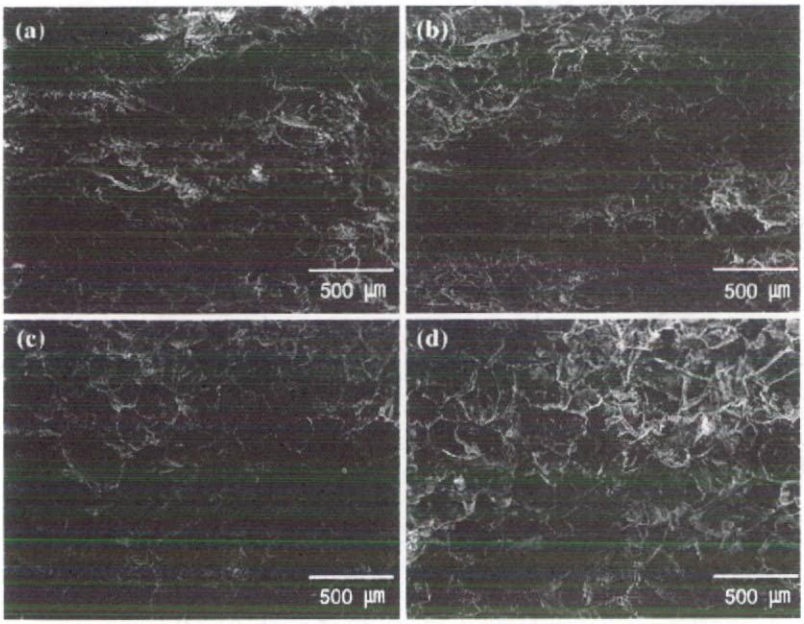

Fig. 5 Scanning electron microscopic observation of the fracture surfaces of $CaCO_3$ bodies under 80 wt.% NaCl. (**a**) 4 MPa molding pressure & 8 h carbonation (**b**) 6 MPa molding pressure & 72 h carbonation (**c**) 8 MPa molding pressure & 72 h carbonation (**d**) 10 MPa molding pressure & 72 h carbonation

expected, it had the lowest mechanical strength. The mechanical strength decreased with the increasing porosity caused by the increase in NaCl content, as shown in Fig. 3b.

We evaluated how much the molding pressure enhances the mechanical strength of the body prepared using 80 wt.% NaCl in the next stage.

Effect of molding pressure under 80 wt.% NaCl

Figure 4a shows the XRD patterns of the composite obtained from the $Ca(OH)_2$/80 wt.% NaCl composite prepared at 10 MPa molding pressure and carbonated for 72 h before and after washing. As shown in Fig. 4a, $Ca(OH)_2$ was not completely transformed into $CaCO_3$ within the

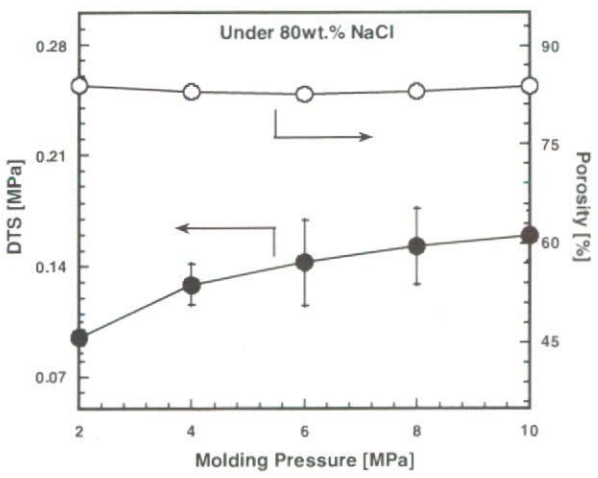

Fig. 6 Changes in diametral tensile strengths and porosities of $CaCO_3$ bodies with molding pressure under 80 wt.% NaCl

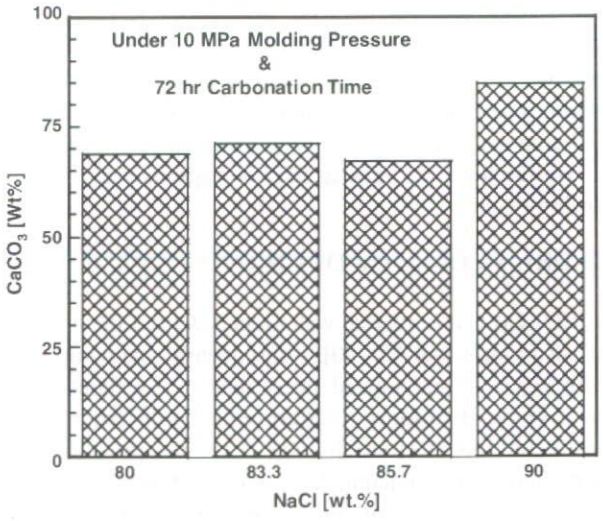

Fig. 7 Changes of $CaCO_3$ content in the $Ca(OH)_2$/NaCl composites at various NaCl content under 10 MPa molding pressure and 72 h carbonation time

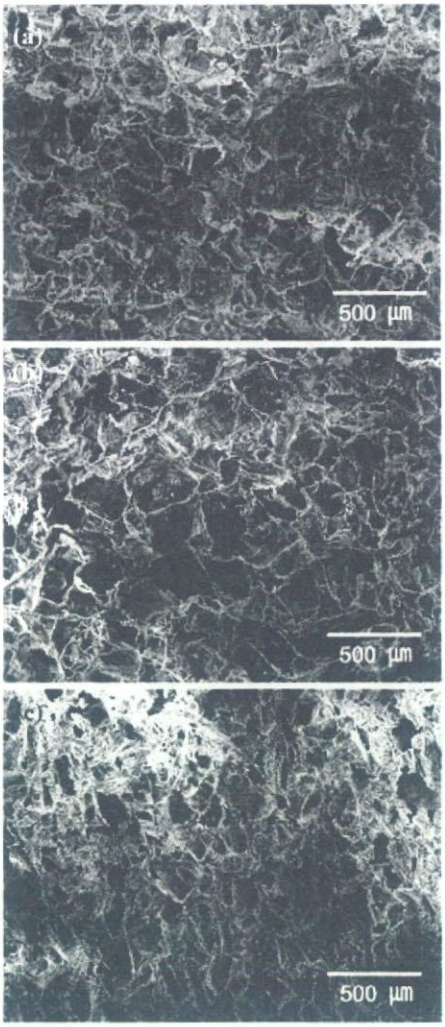

Fig. 8 Scanning electron microscopic observation of the fracture surfaces of $CaCO_3$ bodies after 72 h carbonation under 10 MPa molding pressure. (**a**) 83.3 wt.% NaCl (**b**) 85.7 wt.% NaCl (**c**) 90 wt.% NaCl

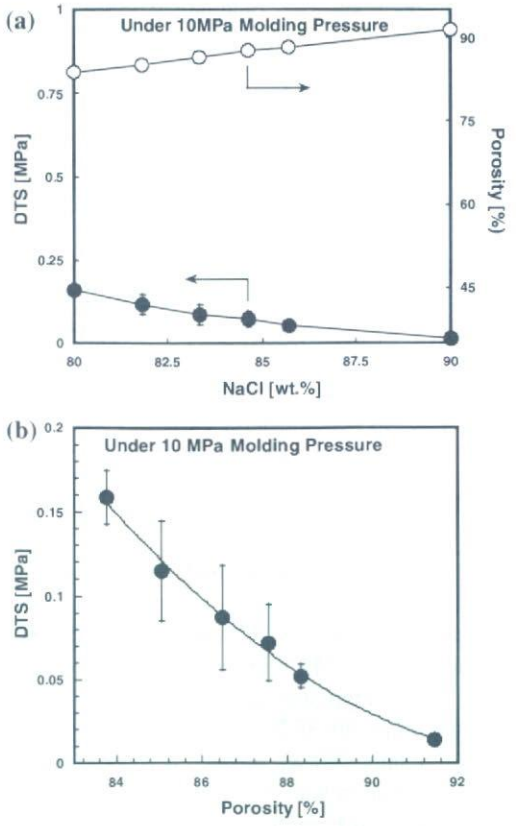

Fig. 9 (**a**) Changes in diametral tensile strengths and porosities of $CaCO_3$ bodies with NaCl content under 10 MPa molding pressure. (**b**) Changes in diametral tensile strengths of $CaCO_3$ bodies with porosity under 10 MPa molding pressure

given carbonation time. However, there was no XRD peak corresponding to $Ca(OH)_2$ in the composite analyzed after washing. Because $Ca(OH)_2$ is soluble in water and, therefore, was removed completely during washing [30]. Fig. 4b shows the degree of carbonation of $Ca(OH)_2$/NaCl composites in terms of molding pressure and time. When the molding pressure was less than 4 MPa, the carbonation of $Ca(OH)_2$/NaCl composite was completed within 8 h. On the other hand, it could not be completed within the given carbonation time when the molding pressure was more than 6 MPa. At the molding pressure of 10 MPa the $CaCO_3$ content in the composite was below 75 wt.%, which was the lowest value under this experimental condition. Actually, the apparent density of $Ca(OH)_2$/NaCl composite prepared at 10 MPa molding pressure was 0.3 g cm^{-3} larger than that of the composite prepared at 2 MPa. Therefore, it is expected that the frame of $Ca(OH)_2$ in the composite and NaCl around this frame was too compact to allow diffusion of CO_2 into the composite or to facilitate carbonation through adsorption of water by NaCl due to high molding pressure

Figure 5 shows the SEM images of fracture surfaces of $CaCO_3$ bodies after carbonation and washing. The average pore size was decreased from 160 μm for 2 MPa (Fig. 2d) to 148 μm for 10 MPa and the average hole size formed in pores also decreased from 49 μm for 2 MPa to 35 μm for 10 MPa, indicating that the body prepared at high molding pressure was dense and compact in comparison with the body prepared at low molding pressure.

Figure 6 shows the changes in the porosity and the mechanical strength of $CaCO_3$ body with molding pressure after carbonation and washing. The apparent density of $Ca(OH)_2$/NaCl composite prepared at 10 MPa molding pressure, as previously mentioned, was higher than that prepared at 2 MPa owing to reduction in the volume of the composite at the molding pressure. Nevertheless, the

porosity of the body was maintained almost the same value regardless of molding pressure, which means that there is no significant change in apparent density of $CaCO_3$ body. The reason for almost constant porosity regardless of decrease in volume of the body can be attributed to the removal of $Ca(OH)_2$ that was not carbonated during washing. We found that, though the porosity was almost constant, the mechanical strength of the body prepared at 10 MPa molding pressure was over 1.5 times as high as that of the body prepared at 2 MPa. This can be regarded as the enhancement of the hardness of frame of the body due to the high molding pressure.

We investigated how much the porosity can be increased under 10 MPa molding pressure by manipulating NaCl content in the following experimental stage.

Effect of NaCl content under 10 MPa molding pressure

Figure 7 shows the degree of carbonation of $Ca(OH)_2$/NaCl composites after 72 h in terms of NaCl content. The degree of carbonation was as low as about 70% in the samples containing 80–85.7 wt.% NaCl, while it was 85% in the one containing 90 wt.% NaCl. It is not clear why the degree of carbonation was the highest at 90 wt.% of NaCl content. However, it is probably due to good dispersion of $Ca(OH)_2$ particles in the NaCl matrix at the high NaCl content. This provides easy access for the penetrated CO_2 gas through the NaCl matrix to $Ca(OH)_2$ and causes a high degree of carbonation.

Figure 8 shows the SEM images of fracture surfaces of $CaCO_3$ bodies after carbonation and washing. The average pore size increased from 148 μm for 80 wt.% NaCl (Fig. 5d) to 177 μm and also the average hole size formed in pores was increased from 35 to 80 μm when NaCl content increased from 80% to 90 wt.%, which means that the hole size is dependent on NaCl content. This result supports the above assumption that the reactive surface area of $Ca(OH)_2$ increases with the increase in NaCl content.

Figure 9a shows the changes in the porosity and the mechanical strength of $CaCO_3$ body with NaCl content after carbonation and washing. The porosity increased with NaCl content under 10 MPa molding pressure. This result shows that the body with over 90% porosity can be prepared by using 90 wt.% NaCl. The mechanical strength decreased with increase in NaCl content. Figure 9b shows a relationship between DTS and porosity. DTS decreases with increasing porosity in a similar way as shown in Fig. 3b obtained at lower porosity region.

Conclusions

It was found that $CaCO_3$ body with macropores over 100 μm can be prepared using NaCl as a water-soluble porogen through this new carbonation method and that these macropores can be interconnected without using any kind of connecting agents. Moreover, the body possessing over 90% porosity can be prepared through this method. The carbonation time necessary to completely transform $Ca(OH)_2$ into $CaCO_3$ can be shortened in the presence of NaCl under relatively low molding pressure. Even though the complete transformation was not achieved within given carbonation time when the high molding pressure was employed, pure $CaCO_3$ body is to be obtained through washing the composite carbonated.

Acknowledgements This work was supported by both Dankook University(DKU-2004-037) and a Grant-in-aid for Scientific Research from the Ministry of Education, Sports, Culture, Science and Technology, Japan.

References

1. Maeda H, Kasuga T, Nogami M, Ueda M (2005) Sci Technol Adv Mater 6:48
2. Miao X, Hu Y, Liu J, Wong AP (2004) Mater Lett 58:397
3. Lemos AF, Ferreira JMF (2000) Mater Sci Eng C 11:35
4. Engin NO, Tas AC (1999) J Eur Cer Soc 19:2569
5. Sous M, Bareille R, Rouais F, Clement D, Amedee J, Dupuy B, Baquey C (1998) Biomaterials 19:2147
6. Piattelli A, Podda G, Scrano A (1997) Biomaterials 18:623
7. Landi E, Tampieri A, Celotti G, Vichi L, Sandri M (2004) Biomaterials 25:1763
8. Suetsugu Y, Takahashi Y, Okamura FP, Tanaka J (2000) J Solid State Chem 155:292
9. Malkaj P, Kanakis J, Dalas E (2004) J Crystal Growth 266:533
10. Tong H, Ma W, Wang L, Wan P, Hu J, Cao L (2004) Biomaterials 25:3923
11. Kasuga T, Maeda H, Kato K, Nogami M, Hata K, Ueda M (2003) Biomaterials 24:3247
12. Manoli F, Kanakis J, Maldaj P, Dalas E (2002) J Crystal Growth 236:363
13. Girot AL, Langlois P, Sangleboeuf JC, Ouammou A, Rouxel T, Gaude J (2002) Biomaterials 23:503
14. Li N, Jie Q, Zhu S, Wang R (2005) Cer Int 31:641
15. Tadic D, Beckmann F, Schwarz K, Epple M (2004) Biomaterials 25:3335
16. Navarro M, Valle SD, Martinez S, Zeppetelli S, Ambrosio L, Planell JA, Ginebra MP (2004) Biomaterials 25:4233
17. Almirall A, Larrecq G, Delgado JA, Martinez S, Planell JA, Ginebra MP (2004) Biomaterials 25:3671
18. Ramay HR, Zhang M (2003) Biomaterials 24:3293
19. Chang BS, Lee CK, Hong KS, Youn HJ, Ryu HS, Chun SS, Park KW (2000) Biomaterials 21:1291
20. Bouler JM, Trecant M, Delecrin J, Royer J, Passuti N, Daculsy G (1996) J Biomed Mater Res 32:603
21. Li SH, Wijn JRD, Layrolle P, Groot KD (2002) J Biomed Mater Res 61:109
22. Sanders JP, Gallagher PK (2002) Thermochimica Acta 388:115

23. Lin X, Matsuya S, Udoh KI, Nakagawa M, Terada Y, Ishikawa K (2003) Archives of Bioceramics Research: Asian BioCeramics Symposium, Fukuoka, Japan vol. 3, p. 83
24. Blom EJ, Nulend JK, Klein CPAT, Kurashina K, Van MAW, Burger EH (2000) J Biomed Mater Res 50:67
25. Bohner M, Lemaitre J, Van PL, Zambelli P, Merkle H, Gander B (1997) J Pharm Sci 86:565
26. Otsuka M, Matsuda Y, Suwa Y, Fox J, Higuchi W (1994) J Pharm Sci 83:611
27. Otsuka M, Matsuda Y, Suwa Y, Fox J, Higuchi W (1994) J Pharm Sci 83:1565
28. Diamond LW, Akinfiev NN (2003) Fluid Phase Equilib 208:265
29. Erdal S, Bahar I, Erman B (1998) Polymer 39(10):2035
30. Elfil H, Roques H (2001) Desalination 137:177

J Mater Sci (2007) 42:7843–7849
DOI 10.1007/s10853-007-1629-3

Characterization of macroporous carbonate-substituted hydroxyapatite bodies prepared in different phosphate solutions

Yoong Lee · Yeong Min Hahm · Shigeki Matsuya · Masaharu Nakagawa · Kunio Ishikawa

Received: 31 July 2006 / Accepted: 20 February 2007 / Published online: 1 June 2007

Abstract Bone mineral of human is different in composition from the stoichiometric hydroxyapatite ($Ca_{10}(PO_4)_6(OH)_2$) in that it contains additional ions, of which CO_3^{2-} is the most abundant species. Carbonate-substituted hydroxyapatite (CHA) bodies were prepared by the hydrothermal treatment of highly porous calcium carbonate ($CaCO_3$) body at 120 °C in 1 M M_2HPO_4 and M_3PO_4 solutions (M = NH_4 or K). It was found that $CaCO_3$ body was almost transformed into CHA body after hydrothermal treatment for 24 h irrespective of type of phosphate solution. However, a small amount of $CaCO_3$ still remained after the treatment in K_3PO_4 for 48 h. Crystal shape of CHA bodies prepared in those solutions except for K_2HPO_4 was flake-like, which was different from that (stick-like) of original $CaCO_3$ body used for the preparation of CHA body. CHA prepared in the K_2HPO_4 showed globule-like crystal. Average pore size and hole size of the CHA bodies were 150, 70 μm and their porosities were about 89% irrespective of the solution. Carbonate content was slightly higher in the CHA bodies obtained from potassium phosphate solutions than in those obtained from ammonium phosphate solutions. Mostly B-type CHA was obtained after the hydrothermal treatment in the potassium phosphate solutions. On the other hand, mixed A- and B-type CHA (ca. 1–2 in molar ratio) was obtained in the ammonium phosphate solutions. The content of CO_3^{2-} in the CHA body depended on the type of phosphate solution and was slightly larger in the potassium phosphate solutions.

Y. Lee (✉) · S. Matsuya · M. Nakagawa · K. Ishikawa
Department of Biomaterials, Faculty of Dental Science, Kyushu University, 3-3-1 Maidashi, Higashiku Fukuoka 812-8582, Japan
e-mail: ly02147@gmail.com

Y. Lee · Y. M. Hahm
Department of Chemical Engineering, College of Engineering, Dankook University, Seoul 140-714, Korea

Introduction

The mineral phase of human hard tissue consists of hydroxyapatite (HA: $Ca_{10}(PO_4)_6(OH)_2$) containing a variety of impurity ions such as carbonate, sodium, and magnesium etc. [1–5]. Carbonate is one of the most abundant impurity ions and its content is about 4–8 wt% [6–8]. In this sense, hard tissue is regarded as carbonate-substituted HA (CHA). It has been reported that synthetic CHA revealed the biological activity better than synthetic HA because the incorporation of carbonate into HA caused an increase in solubility, a decrease in crystallinity, a change in crystal morphology, and an enhancement of chemical reactivity owing to the weak bonding [2, 9, 10]. CHA is actually more soluble in vivo than HA and increases the local concentration of calcium and phosphate ions that are necessary for new bone formation [11–13]. For these reasons, the recent researches have focused on CHA in comparison with HA. Carbonate ion in CHA can be present at two different sites in the apatite lattice [14–18]. One is in hydroxyl site (channel site), called A-type CHA (A-CHA), and the other is in phosphate site, called B-type CHA (B-CHA). These two carbonate types can be distinguished by their infrared spectra: A-type carbonate shows a doublet band at about 1,545 and 1,450 cm^{-1} (asymmetric stretching vibration) and a singlet band at 880 cm^{-1} (out-of-plane bending vibration) and B-type shows the corresponding bands at about 1,455 and 1,410, and 875 cm^{-1},

respectively. A-CHA and B-CHA are abundant in bone of the old and the young, respectively [19]. A-CHA is generally prepared by heating HA at high temperature (800–1,000 °C) under dry carbon dioxide atmosphere as a source of carbonate [19, 20]. In case of B-CHA, it is synthesized by precipitation method and hydrothermal treatment, employing various starting materials. It has been reported that human trabecular osteoclastic cells have low affinity towards A-CHA surface compared to HA [10, 21], whereas B-type substitution can enhance the solubility without changing the surface energy of CHA that affects the initial cell attachment and the collagenous matrix deposition [22, 23]. Even though many researches have been carried out concerning the preparation of CHA, they were related to CHA in the form of powder [7, 9, 16, 19, 20].

In the present study, macroporous CHA bodies were prepared through hydrothermal treatment of porous calcite monolith in various phosphate solutions. The CHA bodies were characterized in terms of chemical and physical properties, such as extent of transformation of $CaCO_3$ body into CHA body, type and content of carbonate and crystal morphology.

Materials and methods

Preparation of CHA body

Calcium hydroxide ($Ca(OH)_2$; Wako Chemicals, Japan) and sodium chloride(NaCl; Wako Chemicals, Japan) were used for the preparation of macroporous $CaCO_3$ body. Ground and sieved NaCl with particle size of 106–300 μm was added to $Ca(OH)_2$ to make a mixture of $Ca(OH)_2$ and 85.7 wt% NaCl. The mixture was put in a stainless steel mold (10 mm in inner diameter) and pressed uniaxially at 10 MPa to prepare $Ca(OH)_2$/NaCl composite. The composite was carbonated in carbon dioxide reaction vessel for 90 h at room temperature. Subsequently, it was washed with distilled water at 90 °C over 3 days to drive off soluble components including NaCl and dried at 60 °C for 24 h. The macroporous $CaCO_3$ body was then treated hydrothermally in 1 M phosphate solutions at 120 °C for various times. Phosphates used are diammonium hydrogen phosphate ($(NH_4)_2HPO_4$; Wako Chemicals, Japan), triammonium phosphate ($(NH_4)_3PO_4 \cdot 3\ H_2O$; Wako Chemicals, Japan), dipotassium hydrogen phosphate (K_2HPO_4; Wako Chemicals, Japan) and tripotassium phosphate (K_3PO_4; Wako Chemicals, Japan). The overall Ca/P molar ratio was 5/9 in which P is three times more than that needed for a stoichiometric HAP formation. Each body after the hydrothermal treatment was washed with distilled water for 6 h to eliminate soluble ions.

Characterization

X-ray diffraction (XRD) analysis

Purity and crystallite size of the CHA formed were determined by XRD (RINT 2500V, Rigaku, Japan) analysis. The XRD pattern was obtained in the range of 2θ from 10 to 60 ° in a continuous mode at a scanning rate of 2 °/min.

Scanning electron microscope (SEM) analysis

Morphology of fracture surface and crystal shape were observed by SEM (JSM 5400LV, JEOL, Japan). Average crystal thickness, average NaCl-print size that can be attributed to the pore size and hole size formed in pore were analyzed by means of image analysis software(USB Digital Scale V1.0, Scalar Corporation).

Fourier Transform Infrared (FT-IR) spectroscopy

Infrared spectra between 400 and 4,000 cm^{-1} were recorded on FT-IR spectrometer (Spectrum 2000, Perkin–Elmer, USA) to examine structural changes by the hydrothermal treatment, in particular, CO_3^{2-} ions substituting for PO_4^{3-} and/or OH^- ions.

Mechanical strength analysis

Compressive strength of the CHA body was evaluated at a constant crosshead speed of 1 mm/min on an universal testing machine (SV-301, IMADA, Japan). Five samples were tested for each experimental condition.

Chemical analysis

Carbon and nitrogen content were determined using CHN elemental analyzer (CHN coder-MT-6, Yanaco, Japan). Calcium and potassium, and phosphorus content were determined by an atomic absorption spectrometer (AAnalyst 300, Perkin–Elmer, Japan) and a spectrophotometer (Ubest-50, Jasco, Japan), respectively.

Porosity measurement

Apparent density was calculated from their weight and dimensions. Relative density was calculated by the ratio of the apparent density to the true density. True density of the $CaCO_3$ body treated hydrothermally for 24 h was measured using a picnometer. The total porosity of the body is defined as follows;

Total porosity(%) = 100(%)–relative density(%)

The total porosity was obtained as the average value of five bodies.

Results and discussion

Figure 1 shows XRD patterns of $CaCO_3$ body after the hydrothermal treatment in the phosphate solutions for various times. Hydroxyapatite (HA) phase was detected as a main reaction product regardless of time and type of phosphate solution. Transformation of $CaCO_3$ into HA in ammonium phosphate solution (c and d) seemed to proceed faster than that in potassium phosphate solution (a and b). With the hydrothermal treatment in ammonium phosphate solutions, transformation of $CaCO_3$ into HA was almost completed even after 6 h. With the potassium phosphate solutions, $CaCO_3$ (peak shown by an arrow) still remained after 6 h. Transformation into HA completed after 24 h in K_2HPO_4, however, a small amount of β-TCP (shown by * in Fig. 1a) was also formed as by-product. On the other hand, though β-TCP was not formed in K_3PO_4 solution, $CaCO_3$ remained even after 48 h, as shown in Fig. 1b. This is probably due to high pH in K_3PO_4 solution, which resulted in stabilization of $CaCO_3$ comparing with carbonate apatite. Actually, solubility difference between both compounds decreased with increasing in pH and almost comparable above pH of 9 [24]. XRD patterns of HA showed a different feature in an extent of separation between (211) and (112) diffraction peaks around 2θ of 32 °. In both of the phosphate solutions, the peaks were well separated in the secondary phosphate solutions comparing with the tertiary phosphate solutions. Those two peaks were almost merged in K_3PO_4 solution. Such a change is often observed when the lattice parameter of a-axis in a hexagonal apatite crystal decreased with increasing in CO_3 content [25]. Table 1 shows the lattice parameter of the apatite phase after the hydrothermal treatment in the phosphate solutions for 24 h calculated from a least square method using the

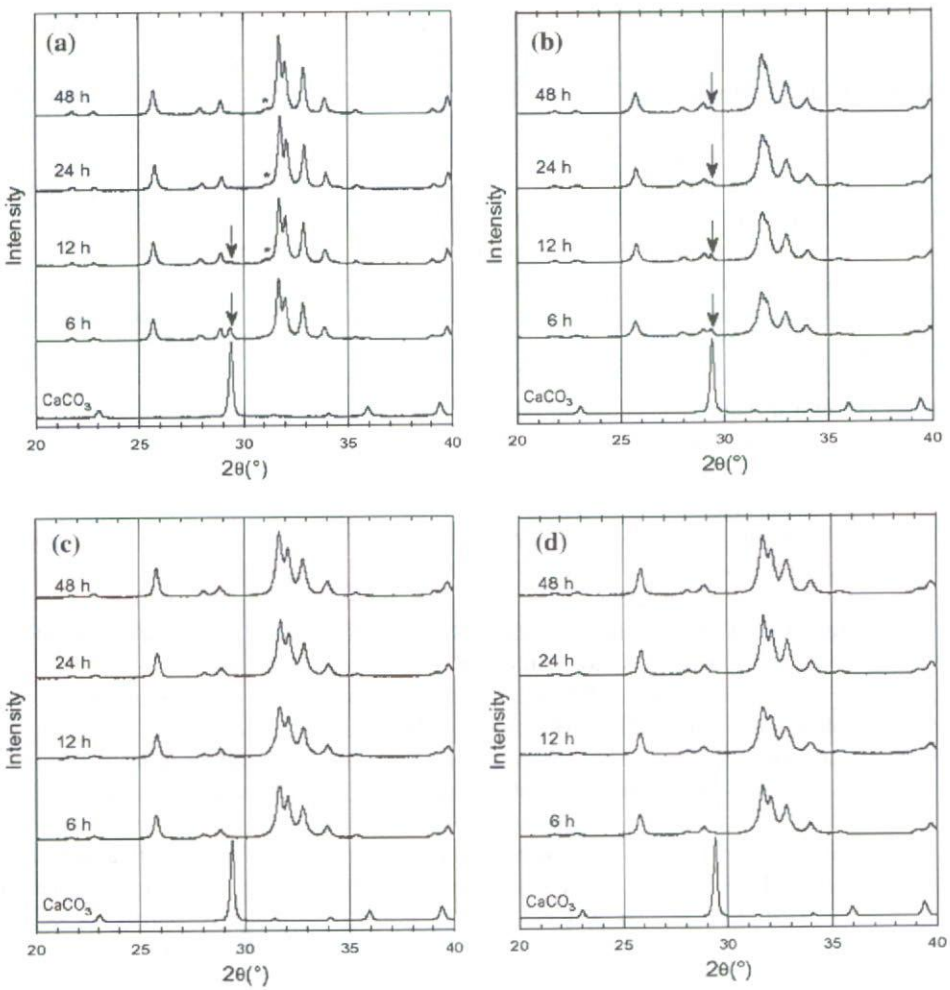

Fig. 1 Change in XRD patterns of CHA bodies hydrothermally treated in various phosphate solutions with time. (**a**) K_2HPO_4, (**b**) K_3PO_4, (**c**) $(NH_4)_2HPO_4$, (**d**) $(NH_4)_3PO_4$

Table 1 Lattice parameters and crystallite size of HA formed after the hydrothermal treatment in various phosphate solutions at 120 °C for 24 h

Solution	Lattice parameter (Å)		Crystallite size (Å)
	a-axis	*c*-axis	
$(NH_4)_2HPO_4$	9.427(0.008)	6.887(0.004)	312
$(NH_4)_3PO_4$	9.439(0.007)	6.894(0.003)	311
K_2HPO_4	9.422(0.008)	6.922(0.004)	601
K_3PO_4	9.386(0.006)	6.904(0.003)	241

diffraction peaks between 10 and 60°. HA formed in K_3PO_4 solution actually showed the smallest *a*-axis parameter among all. It was reported that pure hydroxyapatite showed *a*-axis of 9.421 Å and *c*-axis of 6.88 Å [26]. CHA obtained in the secondary phosphate solutions had almost the same *a*-axis value as the pure hydroxyapatite. However, the CHA obtained in $(NH_4)_3PO_4$ had a larger *a*-axis and that in K_3PO_4 had a smaller one. It is reported that there are two types of CHA, in which PO_4^{3-} lattice site is substituted by CO_3^{2-} (B-type) and OH^- lattice site is substituted by CO_3^{2-} (A-type) [27]. With increasing in CO_3 content of carbonate apatite, *a*-axis increased in A-type CHA and decreased in B-type CHA [28]. The change in *a*-axis described above is closely related to the formation of both type of CHA as discussed later. Crystallinity of HA prepared in K_2HPO_4 solution seems to be the highest, judging from the half width of peaks. Table 1 also shows crystallite sizes of the apatite phase calculated from the half width of the diffraction peaks based on Scherrer's formula [29]. With the ammonium phosphate solution, crystallite sizes of HA were almost the same in both of the slats ($(NH_4)_2HPO_4$: 312 Å, $(NH_4)_3PO_4$: 311 Å). With the potassium solutions, however, crystallite size was much smaller in K_3PO_4 (241 Å) than in K_2HPO_4 (601 Å).

Figure 2 shows FT-IR spectra after the hydrothermal treatment of $CaCO_3$ for 24 h in the phosphate solutions. The typical CO_3^{2-} bands were observed at 1,550–1,400 (ν_3) and 880–870 cm^{-1} (ν_2), and PO_4^{3-} bands at 980–1,100 (ν_3), 960(ν_1) and 560–600 cm^{-1}(ν_4), respectively. There were no peaks of hydrogen phosphate (HPO_4^{2-}, 906, 852 and 530 cm^{-1}) irrespective of types of phosphate solutions [9, 30, 31]. Existence of CO_3^{2-} band in those spectra clearly shows CO_3^{2-}-substituted HA (CHA) formation. B-type CHA shows CO_3 band at about 1,410 and 1,455 cm^{-1}, and A-type at about 1,545 and 1,455 cm^{-1} [32]. With the ammonium phosphate solutions, the CO_3^{2-} band appeared at 1,545, 1,455 and 1,410 cm^{-1}. This observation showed the CHA formed in the ammonium phosphate solutions contained both A-type and B-type CO_3^{2-}. On the other hand, with the potassium phosphate solutions, the band appeared at 1,455 and 1,410 cm^{-1}, which indicates B-type CHA formation. Landi et al. [19] reported that a weight ratio of A- and B-type CO_3^{2-} could be estimated from the intensity ratio of two peaks at 880 and 873 cm^{-1} in the IR spectrum. As shown in Fig. 2b, ν_2CO_3 band was

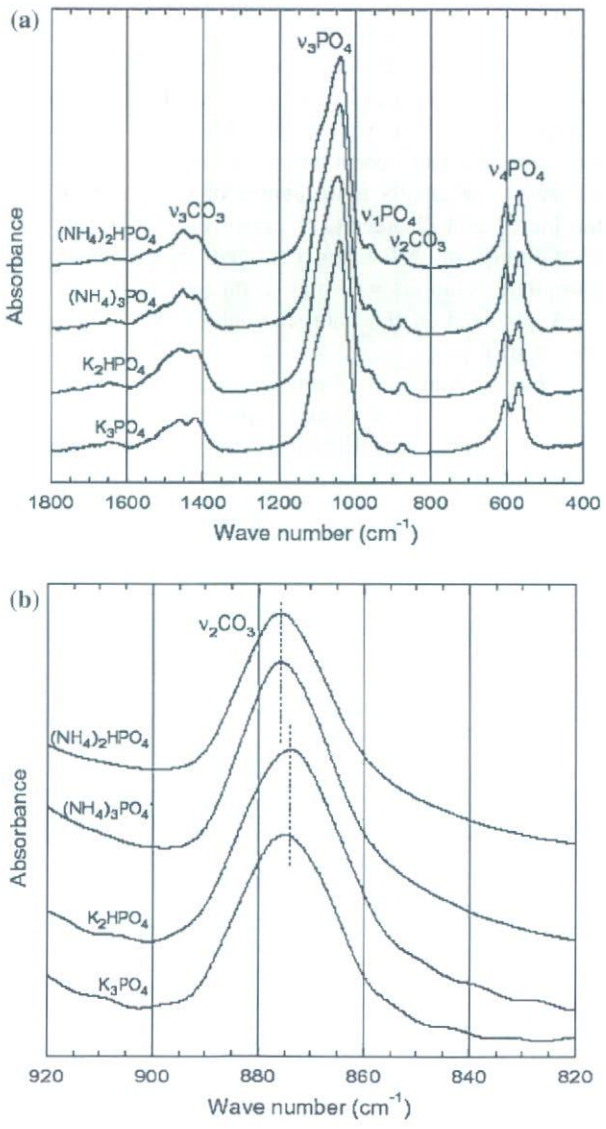

Fig. 2 FT-IR spectra of CHA bodies prepared hydrothermally in various phosphate solutions for 24 h (**a**) and its expanded ν_2CO_3 region (**b**)

observed at slightly higher wave number for the CHA obtained in ammonium phosphate solutions than for that in potassium phosphate solutions. However, the two peaks appeared about 876 and 874 cm^{-1}, which were between the wave number for A-type and B-type CHA. This fact suggests that the peaks consisted of overlapped one of A- and B-type CHA. Therefore we tried to separate the peak graphically using a computer software(Peak Fit, SPSS Inc, Chicago IL, USA). The analysis showed that A/B-type weight ratios were 0.53($(NH_4)_2HPO_4$), 0.54($(NH_4)_3PO_4$), 0.01($hbox{K_2HPO_4}$) and 0 ($hbox{K_3PO_4}$). The result suggests that mixed type CHA (A/B-CHA) was formed in the ammonium phosphate solutions and mostly B-type CHA (B-CHA) was formed in the potassium phosphate solutions. It has been reported that an increase in A-type CO_3^{2-} content in A/B-CHA by means of the migration of B-type CO_3^{2-} to OH^- lattice site with heat treatment caused a decrease in crystallinity, which was attributed to the fact that the hydroxyl site can accept more vacancies and the CO_3^{2-} ion has consequently more degree of freedom that cause the increase in disorder [19]. However, in this study, the crystallinity of A/B-CHA obtained in the ammonium phosphate solutions was high compared with that of B-CHA obtained in the potassium phosphate solutions, as shown in Fig. 1.

Table 2 summarizes chemical composition of the CHA obtained by the hydrothermal analysis for 24 h in various phosphate solutions. OH content was calculated from Eq. (1) on the basis of the electroneutrality condition [4].

$$\frac{\text{wt\% OH}}{M_{OH}} = 2\frac{\text{wt\% Ca}}{M_{Ca}} + \frac{\text{wt\% K[or NH}_4\text{]}}{M_{K[orNH_4]}} - 3\frac{\text{wt\% PO}_4}{M_{PO_4}} - 2\frac{\text{wt\% CO}_3}{M_{CO_3}} \quad (1)$$

M_X in Eq. (1) is the atomic or ionic mass of X. As shown in Table 2, Ca/P ratio showed almost the same value of 1.72–1.73 for the solutions except for K_3PO_4 solution, which had a slightly larger value of 1.84. The CO_3^{2-} content was slightly larger in the potassium phosphate solutions than in the ammonium phosphate solutions. K^+ion was incorporated into CHA more easily than NH_4^+. The main reason for this result can be attributed to the difference in ionic radius between K^+(1.38Å) and NH_4^+ (1.43 Å), meaning that K^+ ions can be more easily replaced with Ca^{2+} (1.00 Å) ions in order to compensate for extra negative charge caused by the substitution of CO_3^{2-} for PO_4^{3-} ions. Chemical formula was obtained based on the chemical composition in Table 2 and A/B CO_3^{2-} ratio from FT-IR analysis and is shown in Eqs. (2)–(5).

$$K_2HPO_4 : Ca_{8.18}K_{0.5}(PO_4)_{4.72}(CO_3)_{1.28}(OH)_{0.1}(CO_3)_{0.02} \quad (2)$$

$$K_3PO_4 : Ca_{8.82}K_{0.42}(PO_4)_{4.79}(CO_3)_{1.21}(OH)_{1.27} \quad (3)$$

$$(NH_4)_2HPO_4 : Ca_{9.23}(NH_4)_{0.12}(PO_4)_{5.36}(CO_3)_{0.64}(OH)_{0.54}(CO_3)_{0.34} \quad (4)$$

$$(NH_4)_3PO_4 : Ca_{9.21}(NH_4)_{0.19}(PO_4)_{5.34}(CO_3)_{0.66}(OH)_{0.18}(CO_3)_{0.36} \quad (5)$$

In the above calculation, it was assumed that PO_4 site has no vacancy, that is, th e total number of subscript ofPO_4^{3-} and CO_3^{2-} ions should be 6. Six types of basic substitution mechanisms have been proposed in literatures [4, 15]. Among these, $Ca^{2+} + PO_4^{3-} + OH^- \Leftrightarrow V_{Ca}$ $CO_3^{2-} + V_{OH}$[mechanism I] and$Ca^{2+} + PO_4^{3-} \Leftrightarrow M^+ + CO_3^{2-}$ [mechanism III] for B-type carbonate substitution was reported as main mechanisms [4]. The chemical formula for B-CHA based on these two mechanisms can be described as follows:

$$Ca_{10-x-y}M_y(PO_4)_{6-x-y}(CO_3)_{x+y}(OH)_{2-x}, \quad (6)$$

where x and y represent the contribution of mechanism I and III, respectively and M stands for alkali or ammonium ion. Main mechanism of A-type carbonate substitution was also proposed as $2OH^- \Leftrightarrow V_{OH} + CO_3^{2-}$ [mechanism V] [19]. If both A- and B-type carbonate substitutions take place simultaneously, the chemical formula for A/B-CHA should be expressed as Eq. (7).

$$Ca_{10-x-y}M_y(PO_4)_{6-x-y}(CO_3)_{x+y}(OH)_{2-x-2z}(CO_3)_z, \quad (7)$$

where z represents the contribution of mechanism V. If x, y and z are calculated using Eq. (6) or (7) from subscript for

Table 2 Chemical composition of CHA prepared by the hydrothermal treatment in various phosphate solutions for 24 h

Phosphate	Ca [wt%]	P [wt%]	Ca/P Molar ratio	NH_4 [wt%]	K [wt%]	CO_3 [wt%]	OH [wt%]
$(NH_4)_2HPO_4$	38.22	17.16	1.72	0.22	–	6.05	0.95
$(NH_4)_3PO_4$	38.18	17.13	1.72	0.34	–	6.3	0.33
K_2HPO_4	34.74	15.5	1.73	–	2.06	8.24	0.18
K_3PO_4	35.86	15.04	1.84	–	1.67	7.39	2.19

CO_3 and K in Eqs. (2) or (3), the values are $0.78(x)$, $0.5(y)$ and $0.02(z)$ for Eq. (2) and $0.79(x)$ and $0.42(y)$ for Eq. (3), respectively. These values gave 8.72 and 1.18 for the subscripts for Ca and OH in Eq. (7), and 8.79 and 1.21 for those in Eq. (8), respectively. The latter subscripts well agreed with those in Eq. (3), however the former did not. This fact suggests that other mechanism also should be taken into account to explain the substitution in the CHA obtained in the K_2HPO_4 solution, besides the above mechanisms. On the other hand, with CHA obtained in the ammonium phosphate solutions, the subscripts for Ca and OH are 9.36 and 0.8 for Eq. (4), and 9.34 and 0.81 for Eq. (5), respectively, when they are calculated in the same way as above. In this case, the former values agreed satisfactorily with the corresponding subscripts in Eq. (4) for CHA obtained in the $(NH_4)_2HPO_4$ solution. The latter values, however, did not agree well, indicating that the other substitution mechanism also should be taken into account again.

Figure 3 shows SEM photographs of CHA obtained in the various phosphate solutions. Crystal shapes of the CHA are quite different from that of the original $CaCO_3$ and largely depend on the type of phosphate solution, as shown in Fig. 3. Most of the CHA crystal showed a flake-like morphology except for the CHA formed in K_2HPO_4. However, crystallite size was much smaller in the CHA obtained in the tertiary phosphate solutions. On the other hand, fine globule-like crystals were formed in the CHA formed in K_2HPO_4 solution (Fig. 3c). A typical fracture surface of the CHA prepared in K_2HPO_4 solution is shown in Fig. 3b.

Those of the CHA prepared in the other solutions also showed a similar structure. Macropores and the holes connecting those pores are seen in the fracture surface. Average pore and hole size were about 150 μm and 70 μm, respectively, irrespective of the type of solutions. Porosity calculated from the relative density was 88–89% in all of the CHA except for the CHA obtained in the K_3PO_4 solution, which was broken into a few pieces during the hydrothermal treatment and didn't keep its original shape. Compressive strength of the CHA was 123 kPa ($(NH_4)_2HPO_4$), 81 kPa ($(NH_4)_3PO_4$) and 64 kPa (K_2HPO_4), which is harder than that (53 kPa) of the original $CaCO_3$ body. The difference in compressive strength

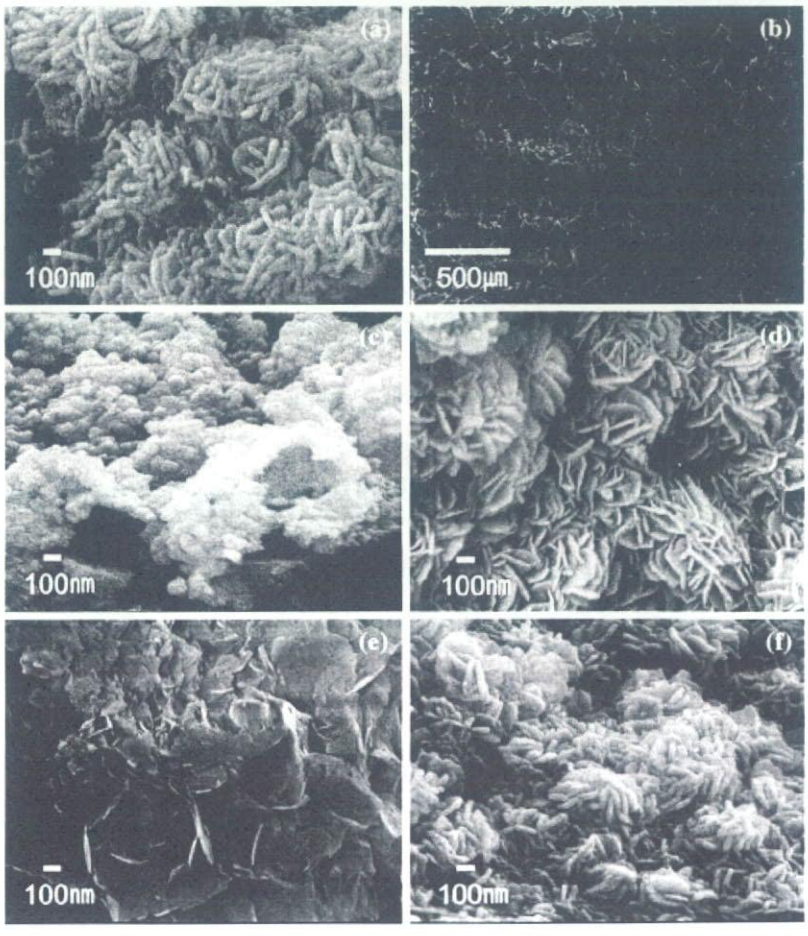

Fig. 3 Scanning electron microscopic observation of $CaCO_3$ and CHA bodies prepared hydrothermally in the various phosphate solutions for 24 h. (**a**) crystal shape of $CaCO_3$ (**b**) fracture surface of CHA prepared in K_2HPO_4 (**c**) crystal shape of CHA prepared in K_2HPO_4 (**d**) crystal shape of CHA prepared in K_3PO_4 (**e**) crystal shape of CHA prepared in $(NH_4)_2HPO_4$ (**f**) crystal shape of CHA prepared in $(NH_4)_3HPO_4$

for the CHA is presumably related to the difference in crystallite size and crystal shape because other properties, such as porosity and average pore and hole size, are similar each other.

Conclusions

CHA, carbonate-substituted hydroxyapatite, bodies were prepared by the hydrothermal treatment of pure $CaCO_3$ body at 120 °C in secondary and tertiary ammonium or potassium phosphate solutions. Transformation of $CaCO_3$ into CHA was almost completed by the hydrothermal treatment for 24 h except for K_3PO_4 solution, in which a small amount of $CaCO_3$ remained even after 48 h. Carbonate content of the CHA was slightly higher with potassium phosphate solutions than with ammonium phosphate solutions. Mostly B-type CO_3^{2-} substitution takes place when $CaCO_3$ body is treated hydrothermally in the potassium phosphate solutions. On the other hand, mixed A- and B-type CHA was obtained in the ammonium phosphate solutions. The content of CO_3^{2-} in the CHA body depended on the type of phosphate solution. The average pore and hole size were about 150 and 70 μmin all of the solutions.

Acknowledgements This study was supported in part by a Grant-in-aid for Scientific Research from the Ministry of Education, Sports, Culture, Science, and Technology, Japan

References

1. Rau JV, Cesaro SN, Ferro D, Barinov SM, Fadeeva JV (2004) J Biomed Mater Res Part B: Appl Biomater 71B(2):441
2. Baig AA, Fox JL, Su J, Wang Z, Otsuka M, Higuchi WI, Legeros RZ (1996) J Colloid Interface Sci 179:608
3. Tang R, Henneman ZJ, Nancollas GH (2003) J Cryst Growth 249:614
4. Rieters IY, Maeyer EAPD, Verbeeck RMH (1996) Inorg Chem 35:5791
5. Wenk HR, Heidelbach F (1999) Bone 24(4):361
6. Landi E, Tampieri A, Celotti G, Langenati R, Sandri M, Sprio S (2005) Biomaterials 26:2835
7. Barralet J, Best S, Bonfield W (1998) J Biomed Mater Res 41(1):79
8. Barralet J, Akao M, Aoki H (2000) J Biomed Mater Res 49(2):176
9. Suchanek WL, Shuk P, Byrappa K, Riman RE, Tenhuisen KS, Janas VF (2002) Biomaterials 23:699
10. Redey SA, Nardin M, Assolant DB, Rey C, Delannoy P, Sedel L, Marie PJ (2000) J Biomed Mater Res 50(3):353
11. Barralet JE, Aldred S, Wright AJ, Coombes AGA (2002) J Biomed Mater Res 60:360
12. Matsumoto T, Okazaki M, Inoue M, Ode S, Chien CC, Nakao H, Hamada Y, Takahashi J (2002) J Biomed Mater Res 60:651
13. Barralet JE, Best SM, Bonfield W (2000) J Mater Sci: Mater Med 11:719
14. Tonsuaadu K, Peld M, Leskela T, Mannonen R, Niinisto L, Veiderma M (1995) Thermochim Acta 256:55
15. Feki HE, Savariault JM, Salah AB, Jemal M (2000) Solid State Sci 2:577
16. Oliverira LM, Rossi AM, Lopes RT (2000) Appl Radiat Isotopes 52:1093
17. Fleet ME, Liu X (2004) J Solid State Chem 177:3174
18. Fleet ME, Liu X, King PL (2004) Am Mineral 89:1422
19. Landi E, Tampieri A, G Celotti, Vichi L, Sandri M (2004) Biomaterials 25:1763
20. Fleet ME, Liu X (2003) J Solid State Chem 174:412
21. Redey SA, Razzouk S, Rey C, Assollant DB, Leroy G, Nardin M, Cournot G (1999) J Biomed Mater Res 45:140
22. Ellies LG, Lelson DGA, Featherstone JDB (1988) J Biomed Mater Res 22:541
23. Navarro M, Valle SD, Martinez S, Zeppetelli S, Ambrosio L, Planell JA, Ginebra MP (2004) Biomaterials 25:4233
24. Verveecke G, Lemaitre J (1990) J Cryst Growth 104:820
25. Legeros RZ, Trautz OR (1967) Science 155:1409
26. Legeros RZ (1991) In: Meyers HM (ed) Monographs in oral science, vol 15. KARGER, Basel, p 18
27. Bonel G, Montel G (1964) Comp Rend Acad Sci (Paris) 258:923
28. Legeros RZ (1991) In: Meyers HM (ed) Monographs in oral science, vol 15. KARGER, Basel, p 89
29. Cullity BD (1978) Elements of X-ray Diffraction, 2nd edn. Addison-Wesley Pub Co Inc, Philippines, p 102
30. Bouhaouss A, Bensaoud A, Laghzizil A, Ferhat M (2001) Int J Inorg Mater 3:437
31. Dekker RJ, Bruijn JDD, Stigter M, Barrere F, Layrolle P, Blitterswijk CAV (2005) Biomaterials 26:5231
32. Elliott JC (1994) Structure and chemistry of the apatites and other calcium orthophosphates. Studies in Inorganic Chemistry 18, Elsevier, Amsterdam, pp 230–234